Published in final edited form as:
Magn Reson Imaging. 2011 June ; 29(5): 587–600. doi:10.1016/j.mri.2011.02.003.

Magnetic Resonance in the Era of Molecular Imaging of Cancer

John C. Gore, **H. Charles Manning**, **C. Chad Quarles**, **Kevin W. Waddell**, and **Thomas E. Yankeelov**
Vanderbilt University Institute of Imaging Science

Abstract

MRI has played an important role in the diagnosis and management of cancer since it was first developed, but other modalities also continue to advance and provide complementary information on the status of tumors. In the future there will be a major continuing role for non-invasive imaging in order to obtain information on the location and extent of cancer, as well as assessments of tissue characteristics that can monitor and predict treatment response and guide patient management. Developments are currently being undertaken that aim to provide improved imaging methods for the detection and evaluation of tumors, for identifying important characteristics of tumors such as the expression levels of cell surface receptors that may dictate what types of therapy will be effective, and for evaluating their response to treatments. Molecular imaging techniques based mainly on radionuclide imaging can depict numerous, specific, cellular and molecular markers of disease and have unique potential to address important clinical and research challenges. In this review we consider what continuing and evolving roles will be played by MRI in this era of molecular imaging. We discuss some of the challenges for MRI of detecting imaging agents that report on molecular events, but highlight also the ability of MRI to assess other features such as cell density, blood flow and metabolism which are not specific hallmarks of cancer but which reflect molecular changes. We discuss the future role of MRI in cancer and describe the use of selected quantitative imaging techniques for characterizing tumors that can be translated to clinical applications, particularly in the context of evaluating novel treatments.

Introduction

Magnetic resonance imaging and spectroscopy of human subjects *in vivo* have enjoyed over 30 years of steady progress. Today, MRI is well established as the single most useful imaging modality available in radiological practice, especially for the detection and characterization of soft tissue pathologies such as solid tumors in cancer. MRI produces exquisite three dimensional images non-invasively, with high spatial resolution and high contrast, and the quality and acquisition times of images continue to improve as technological innovations such as parallel imaging [1], compressed sensing [2] and higher field strengths [3] are introduced. However, in parallel with these developments, other modalities (most notably X-ray CT, ultrasound and nuclear imaging) have also shown dramatic advances, and improvements in one diagnostic technique seem often to catalyze improvements in other domains. Moreover, the applications of imaging technologies have also evolved from traditional radiological diagnosis to addressing other types of problem in

Address for Correspondence: Dr. John C. Gore, Vanderbilt University Institute of Imaging Science, AA1105 MCN, 1161 21st Ave South, Vanderbilt University, Nashville, TN 37232-2310, Tel: (615) 322 8359, john.gore@vanderbilt.edu.

biomedical research and patient management. Current trends in the use and nature of imaging build on developments in other fields such as genomics and molecular biology, and the types of application and procedures have changed from those of even a few years ago. For example, imaging is increasingly used to assess function rather than just anatomy (e.g. for studies of the brain), or to characterize individual phenotypes for targeted drug therapies. Much greater use is made of quantitative measurements from images rather than subjective judgements, and pre-clinical imaging of animal models of disease has increased dramatically with the development of specialized instrumentation. Of particular note has been the emergence of molecular imaging to assess specific cellular and molecular processes in living tissues. Figure 1 depicts the growth of molecular imaging, over the past decade, as measured by the number of records each year reported by searching PubMed. Molecular imaging is often conceived to be the province of nuclear and optical imaging methods because of their great sensitivity for detecting probes that may be designed to report on specific molecular targets. Nonetheless, MRI will continue to be of major relevance as translational molecular techniques are developed, and thus it is timely to consider what specific capabilities MRI is likely to contribute in the era of molecular imaging, particularly for the detection and characterization of cancer.

It is instructive to appreciate precisely how far and how fast MRI has advanced in the last three decades. Figure 2 shows an early *in vivo* image of the human brain acquired at 0.15T in 1984 and a similar section acquired at 7.0T in 2008. There clearly has been a remarkable increase in spatial resolution, speed and signal to noise ratio, and these have enabled multiple new types of applications. Much of the improvement in image quality has been derived directly from using stronger magnetic fields and improved gradient and radiofrequency coils. Moreover, the range and types of information available from MR methods has also continued to increase. MR images may provide excellent contrast because of variations in water proton density, relaxation times (which reflect macromolecular content), molecular Brownian motion (diffusion imaging), flow, the effects of contrast agents, chemical composition (e.g. concentration of amides or lipids, or metabolites), and even mechanical properties such as elastic constants and strain rates. Figure 3 shows a selection of such images, all of which qualify as “MR images”, produced by a standard, modern clinical scanner. MRI thus connotes a class of images that can portray a range of types of information available using the same instrumentation. We consider below how this rich array of information may evolve in the era of molecular imaging.

Molecular Imaging

The Society of Nuclear Medicine has defined molecular imaging;

“ Molecular imaging is the visualization, characterization, and measurement of biological processes at the molecular and cellular levels in humans and other living systems. Molecular imaging agents are probes used to visualize, characterize and measure biological processes in living systems. Both endogenous molecules and exogenous probes can be molecular imaging agents ” [4].

As we will argue “*characterization ..... of biological processes at the....cellular level”* is an area in which MRI can excel, especially via the development and application of quantitative imaging biomarkers. “Biomarker” is a term used widely in drug development and is defined as “a characteristic that is objectively measured and evaluated as an indicator of normal biological processes, pathogenic processes, or pharmacologic responses to a therapeutic intervention” [5]. Much imaging research can be considered the development of imaging biomarkers. For example, the uptake of glucose as measured in FDG-PET may be considered an indirect biomarker of metabolism, which is often different between normal

and abnormal tissues and after a treatment. Imaging biomarkers are likely to be very useful in clinical management, especially to assess whether a patient is likely to respond to a treatment, or to detect and evaluate the treatment response.

To identify potential imaging biomarkers in oncology, it is useful to consider specific questions relevant to cancer that we may wish to address by different imaging methods. For example, we may wish to characterize the phenotype and state of some solid tumors by assessing, for example, the blood perfusion and/or oxygenation of the tissue, both of which are highly relevant in considering certain classes of therapy. We may wish to assess whether specific therapeutic targets (e.g. EGFR, VEGF, HER2) are over-expressed by the tumor, and whether a targeted drug or antibody actually changes this level of expression. We also want to know early in the course of therapy whether a tumor responds to the treatment, before there are gross changes in tumor size or clinical manifestations.

Biomarkers may be based on assessing molecular events and cellular characteristics directly, by detecting, for example, changes in the number of specific receptors or synthetic pathways that are altered in malignancy; or they may measure more “downstream” effects on tumor physiology, metabolism, and biophysics, such as changes in cell density or blood flow. The former are well suited for nuclear imaging, and much current research in PET aims to address such challenges, but here we argue that the latter are well suited for MRI. These differences may be illustrated by considering some specific measurements of potential interest. We can assess the physiological and biophysical status of tissue by measuring properties such as tumor size (the basis of the current imaging metrics of response in clinical trials, using the RECIST [6] criteria), rate of proliferation and cellularity, metabolism (glycolysis, whether anerobic or aerobic, or uptake and usage of other substrates such as glutamine or choline), oxygenation (pO_2 and degree of hypoxia), or vascular properties (blood flow, blood volume, or vascular permeability). These characteristics are not tumor-specific but they are important indicators of the state of any tissue, and changes within them are usually “downstream” sequelae of treatment effects or other changes in molecular or cellular processes. Other features such as biochemical tumor-host Interactions, or changes in extracellular matrix signaling, cell surface receptors, intercellular signaling pathways, and gene expression, are more “molecular” in nature and are better suited to nuclear imaging methods. Thus, we suggest that the “measurement of biological processes at the molecular and cellular levels” translates for MRI to using quantitative imaging biomarkers that report *indirectly* on molecular or cellular changes in tissue: for example, increases/decreases in cell density are an indirect biomarker of changes in proliferation or apoptosis, reductions in vascularity are a biomarker of anti-angiogenic effects, and increased lactate production may be a biomarker of anerobic metabolism. We illustrate these issues further by considering some specific MRI methods that are already being used in clinical trials.

Cellularity and Diffusion Imaging

Increased and unregulated rates of cell proliferation are a hallmark of aggressive tumors. A direct molecular approach for assessing proliferation is the use of 3′-deoxy-3′-(18)F-fluorothymidine ([18]FLT-PET), which measures the activity of the enzyme thymidine kinase 1 as cells undergo division. On the other hand, an “indirect” MR approach is Diffusion Imaging which measures the consequences of proliferation. Rapid cellular proliferation leads to increased cell density and tumor growth. Diffusion MR Imaging measures the consequences of proliferation and thus under appropriate circumstances may be used as a quantitative biomarker of cellularity. MR imaging methods that are sensitive to the rate of diffusion of water molecules (diffusion weighted imaging (DWI)) can provide novel information on tissue cellularity that is not obtainable by other means, and which is now being used in studies of tumors and their response to therapy.

Conventional MRI detects signals (mainly) from tissue water molecules which are constantly undergoing random Brownian motion. As a result, the mean squared displacement of each molecule from its starting position increases linearly with time, and the rate of increase is proportional to the self-diffusion coefficient *D*. In free water at 37 degrees C, $D \approx 3\times10^{-5}$ cm^2sec^{-1}, so water molecules typically would migrate about 13.4 microns in any direction in a time of 30 milliseconds at body temperatures. However, in tissues the value of *D* is found to be much lower than in free solutions because of restrictions on free diffusion caused by, for example, cell membranes that are not fully permeable and which hinder the water molecules mobility. In this case the measured displacements are reduced and the process is described by an *apparent diffusion coefficient* or ADC [7].

ADC values for tissue water can be measured quantitatively by acquiring sets of images with different imaging parameters. Usually DWI is performed by incorporating additional magnetic field gradients into the MRI acquisition, which serve to attenuate the MR signal to a degree that depends on the ADC and the gradient strength. By acquiring and comparing images with different values of the gradient strength, the ADC can be explicitly calculated and maps of ADC can be calculated.

From numerous studies, including work in packed cells [8], it is apparent that conventional measurements of diffusion using MRI report values of ADC that vary inversely with cell density. DWI have thus been used to infer tumor cellularity [9,10]. Cellularity is a term usually used to describe the density of cells within a tumor, or region of tumor, and often correlates with the aggressiveness of the tumor's growth. Regions with high cellularity are often indicative of rapid cell division and tumor growth, while necrotic regions of tumors, which may form in the wake of rapid growth or in response to treatment, exhibit low cellularity. A quantitative map of tumor cellularity, acquired in vivo, may be a valuable tool for both treatment planning and monitoring. Several early studies revealed abnormal water diffusion in various tumors [11 – 15] but more detailed quantitative relationships between microstructure and ADC have only recently been explored. ADCs were first shown to change in response to tumor treatment by Zhao et al. [16] who measured water ADC in excised RIF-1 tumors following treatment with an anti-cancer drug. These data revealed that the ADC increase began while the tumors were still growing, suggesting it could be an early indicator of favorable cytotoxic treatment response. Other studies followed which show ADC changes in experimental tumors following treatment with drugs or gene therapy [17 – 22]. Water ADCs have also been shown to correlate specifically with cell density in a variety of tumor models [9, 10, 23]. Further details on these and other studies of water ADCs in tumors can be found in recent review papers [24, 25]. Figure 4 shows an example of how ADC maps in a mouse tumor model change (residual tumor values generally increases) after successful treatment with a cytotoxic drug.

In human studies to date, higher pre-treatment ADC values generally tend to correlate with poorer response to therapy and prognosis [26 – 28]. For example, in a recent study characterizing hepatic metastases with DWI, thirty-eight responding and forty-nine non-responding lesions were evaluated in patients with confirmed metastases originating from gastrointestinal cancers [28]. In these patients, the mean pre-therapy ADC for non-responding lesions was found to be significantly higher than that of non-responding lesions. Similarly, in a study reporting a smaller group of patients presenting with colorectal hepatic metastases, Koh et al. found that higher pre-treatment ADC values were predictive of poor response to chemotherapy [27].

For quantitative assessment of therapeutic regimens, early responses to various interventions have correlated with increasing ADC values in many studies. Representative reports illustrating increased ADC in correlation with ultimate tumor response following early

intervention include studies involving human brain tumors [29], brain tumor animal models [30], prostate metastases to bone [31], human breast tumors [32], mouse models of breast cancer [33,34], primary rectal tumors [26], CRC hepatic metastasis [27,28], and mouse models of CRC [35]. The majority of these studies have been performed in combination with either cytoxic drugs and/or radiation. The observed increase in ADC values following therapy appears to be a generalized phenomenon and can stem from a number of cell death mechanisms including apoptosis [34], lytic necrosis, authophagy, and/or mitototic catastrophe [33]. Because water within tumor cells is in a restricted environment relative to extracellular water, loss of cell membrane integrity and cellular density resulting from any or all of these cell death mechanisms could play a role in the observed changes in ADC following therapy. Recent studies in preclinical models have illustrated observable ADC changes following treatments resulting in primarily apoptosis [34] as well as preclinical models where non-apoptotic cell death mechanisms predominate [33]. Many tumors can rapidly outgrow their vascular and nutrient supply, so extreme metabolic stress as well as drastic changes in hypoxia and pH can induce progressively substantial central necrosis, with expected concomitant changes in the ADC.

Vascularity and DCE-MRI

When a malignant tumor reaches approximately one mm^3 in volume, it can no longer rely on the passive diffusion of metabolites from host tissue blood vessels to be able to continue to proliferate, so new vasculature must develop in order for the tumor to continue to thrive. In such circumstances, tumors release various proteins which migrate to existing vasculature and cause these vessels to change. Paramount among these proteins are the vascular endothelial growth factors (VEGFs), which cause the endothelial cells that form existing vessels to grow, proliferate, and migrate up the VEGF concentration gradient; i.e., towards the growing tumor. This process of neovacularization is the well-known phenomena of angiogenesis [36]. It is believed that virtually all tumors are dependent upon angiogenesis for survival, and various chemotherapeutic drugs are designed to interfere with angiogenesis, so a method for imaging and quantitatively assessing this phenomena would potentially have a useful role in clinical oncology.

The direct molecular approach to assessing angiogenesis might well be to label and detect the tissue expression or binding of molecules such as VEGF. However, MRI provides a less direct but very informative method for assessing vascular changes in tumors. In contrast to blood vessels that are the result of normal physiologic processes, tumor vessels produced by angiogenesis are characteristically leaky, fragile, and incompletely formed. These differences may be exploited in order to characterize the neovasculature and, indirectly, the state of the tumor. Dynamic contrast enhanced magnetic resonance imaging (DCE-MRI) measures the density, integrity and leakiness of tissue vasculature. Changes in the parameters obtained by DCE-MRI can be used to assess how a tumor is responding to treatment. The method is based on measurements and mathematical models of how a paramagnetic tracer perfuses through such vessels. It is a reasonable hypothesis that healthy vessels in normal tissues may be characterized by a range of parameters measuring blood flow, vessel permeability, and tissue volume fractions (i.e., fractions of a given sample of tissue that can be attributed to intravascular or extravascular space). Similarly, it is plausible that some or all of these parameters will be different in pathologic vessels. In recent years, there has therefore been great interest and considerable development in the use of DCE-MRI to study these phenomena.

DCE-MRI involves the serial acquisition of MR images of a tissue of interest (e.g., a tumor) before, during, and after an intravenous injection of a paramagnetic contrast agent (CA), which alters the MR signals from tissues by reducing the inherent NMR relaxation time, T_1,

which describes the time of recovery of the tissue's longitudinal magnetization back towards equilibrium. By acquiring a set of images before, during, and after injection of the agent, each image voxel displays a signal intensity time course which can be related to the agent's concentration. This time course can then be analyzed with an appropriate mathematical pharmacokinetic model. By fitting the DCE-MRI data to such a model, physiological parameters can be extracted that relate to, for example, tissue perfusion, microvascular vessel wall permeability, and extracellular volume fraction (reviewed in [37]). Much recent work has focused on use of the parameter K^{trans}, which represents the product of the permeability and the vascular epithelial surface area from which the agent leaks into tissue. It has been shown that both healthy and pathologic tissues exhibit characteristic signal intensity time courses as well as pharmacokinetic parameter values. Furthermore, because these parameter values are probes of tissue status, they may be used to differentiate malignant from benign tumors, aid in tumor staging, and monitor treatment response.

Li et al. [38] applied this type of approach to follow the effects of AG-013736, a novel vascular endothelial growth factor receptor tyrosine kinase inhibitor on tumor xenografts. They found that the transfer constant afforded by DCE-MRI analysis was able to successfully separate control from treated groups. Numerous reports have appeared in recent years of similar successful applications of DCE-MRI (for example, [39 – 43])

DCE-MRI has also been used extensively within the clinical setting to assess tumor response to treatment. Figure 5 (top row) depicts K^{trans} maps overlaid on T_1-weighted SPGRE image acquired before treatment (panel a), after one cycle of neoadjuvant chemotherapy (panel b) and at the conclusion of a therapy but prior to surgery. This is an example of patient showing a complete clinical response. The bottom row shows similar data for a patient exhibiting progressive disease. Notice how, in the top panel, there is a general decrease in K^{trans} values from pre- to post-one cycle of therapy (panels a and b, respectively), whereas in the bottom row there is a general increase (panels d to e) and this correlates with disease burden at the time of therapy. As there are many treatment paradigms currently available for a variety of cancers, an important clinical need is to develop a noninvasive method to determine if a therapy is effective. Thus, a central goal of many quantitative DCE-MRI studies is to determine, early in the course of therapy, if pharmacokinetic parameters can be predictive of treatment response. Ah-See *et al* [44] evaluated 28 patients with breast cancer for response (11 pathologic responders and 17 non-responders) by DCE-MRI obtained after two cycles of neoadjuvant 5-fluorouracil, epirubicin, and cyclophosphhamide chemotherapy. While a number of pharmacokinetic parameters were evaluated (including those listed above), they found that K^{trans} was the best predictor of pathologic response with area under the ROC curve of 0.93 providing a sensitivity and specificity of 94% and 82%, respectively, which translated into correctly identifying 94% of non-responders and 73% of responders. Just as in the pre-clinical arena, there is by now a well-developed literature reporting similar successes (for example, [45 – 49]).

A related emerging approach to interrogate the tumor vascular and hemodynamic status is Dynamic Susceptibility Contrast MRI (DSC-MRI), which, like DCE-MRI, relies upon the serial acquisition of images after the injection of a contrast agent. Unlike DCE-MRI, which detects changes in a tissue's T1 relaxation time, DSC-MRI measures contrast agent induced alterations in the native transverse relaxation times, T2 and T2*. The acquired DSC-MRI data are then fit to an appropriate pharmacokinetic model to extract parameters relating to blood volume, blood flow and mean transit time. The relationship between the DSC-MRI signal change and CA concentration is not as straightforward as in DCE-MRI because it depends upon the underlying geometry of the CA distribution in tissue (e.g. within vessels or surrounding cells). The effective relaxivity (change in relaxation rate per concentration) can be quite variable, and depends on the sizes, concentrations and arrangement of the

compartments containing the agent [50], which may fundamentally affect the reliability of measurements made by this technique. In practice, these considerations are usually ignored, the geometrical contributions are assumed to be constant across tissue types, and the derived CA concentration time series and kinetic parameters are considered relative values. Despite this potential confounding factor DSC-MRI derived maps of relative tumor blood flow and blood volume have exhibited a correlation with brain tumor grade [51 – 54] and treatment response [55 – 57]. Further, the applicability of DSC-MRI to non-cerebral tumors (e.g. breast and prostate) is currently under investigation [58. 59]. A potential advantage of DSC-MRI's sensitivity to the underlying CA distribution geometry is that it can be used to extract additional features of the tumor tissue such as mean vessel diameter [52, 60] or intercellular distances [61]. The simultaneous assessment of morphological and functional features of the tumor circulation makes DSC-MRI a powerful approach for the non-invasive characterization of the tumor microenvironment.

Direct Molecular Imaging Approaches using MRI

Although the examples above demonstrate the utility of indirect approaches to measurements of changes in molecular processes in tissues, many investigators have attempted to perform more direct molecular imaging studies using MRI. Two distinct approaches to detecting molecular imaging probes by MRI are possible. The first of these is direct detection of a nuclear species that is a component of an imaging probe (e.g., nuclei of ^{19}F, ^{2}H, or ^{13}C within molecules introduced into the body). The second approach is indirect detection via the effects of an agent on the large signal available from the hydrogen nuclei (protons) in tissue water, either by changing the water relaxation rate or by introducing new pathways for magnetization transfer.

The direct approach is most comparable to radionuclear imaging. However, detecting nuclei on the basis of NMR is much less sensitive than counting emitted high-energy photons,. The nuclear magnetization within the sample determines the maximum signal obtainable, and at body temperature is limited because at common fields approximately only 5 in 1,000,000 of the nuclei contribute to the net signal (though for some nuclei this sometimes can be increased via hyperpolarization as described below). The most promising prospect for direct imaging without hyperpolarization is ^{19}F (e.g., in perfluorocarbons). Fluorine has the largest gyromagnetic ratio after hydrogen and thus at a given field strength and concentration produces stronger signals than any other species. Because no background fluorine signal exists under normal physiologic conditions, detection of the presence of an agent requires merely that the measured signal be greater than the ambient level of noise, the random fluctuations in the apparent image background. However, unlike the cases for nuclear and x-ray imaging, the background noise variance in MRI is essentially independent of the signal (not counting "structured noise" such as motion effects, which can be signal-related) and is therefore the same magnitude for fluorine as for protons. Thus, the sensitivity for detecting small amounts of fluorine (by contrasting a small positive increase relative to the background noise) does not differ much from the sensitivity for detecting small variations in the large proton background caused, for example, by relaxation agents, or the presence of various metabolites containing protons. Multiple experiments with in vivo MR spectroscopy have established that in practice at common field strengths, the lower limit on the total amount of the detectable species is approximately 1 micromole with adequate signal-to-noise ratio (SNR) and in reasonable times [62]. The necessary tissue concentration depends on the number and sizes of the imaging voxels. For example, approximately a 1 μM concentration is detectable from a 1 liter volume (e.g. whole brain), whereas 1 mM is the required concentration when measurements are made from a 1 mL voxel. For in vivo MR spectroscopic estimates of major metabolites such as N-acetyl aspartate and choline, spectral images of dimension about 1mL are typically acquired in reasonable times with an SNR of

more than 30 [63]. To achieve molecular imaging with, for example, fluorine at a spatial resolution of 2 × 2 × 5 mm, the volume-averaged concentration of fluorine atoms within the voxel must then be on the order of 50 mM for the same SNR, and proportionately less (≈ 5 mM, corresponding to an amount of 100 nanoMoles) for mere detection above the noise.

For the second of these approaches, either of two concepts may be used: using paramagnetic or superparamagnetic agents that alter the tissue proton relaxation time T1, T2, or T2* (the basis of conventional MRI contrast agents), or manipulating the magnitude of the water signal via specially designed radiofrequency irradiation that labels one species of protons (e.g., by selectively saturating the magnetization of protons within a specific chemical group) that in turn transfer the label to the water via magnetization exchange. This is the basis of so-called CEST (chemical exchange saturation transfer) and PARACEST (paramagnetic chemical exchange saturation transfer) agents [64].

In general the design of MR contrast agents may be classified into four different types for different applications. These are (1) nonspecific contrast agents, such as the commonly used lanthanide chelates or intravascular blood pool agents, which do not incorporate any specific targeting strategies [65, 66]; (2) targeted contrast agents, which are usually paramagnetic species attached to or part of specifically engineered molecules, such as antibodies, which are directed toward and taken up by specific molecular targets [67.68]; (3) so-called “smart” contrast agents, which do not rely on selective targeting to achieve spatial specificity but instead change their efficacy (and thus their effects on the MR signal) only in response to specific local molecular characteristics (e.g., the presence of specific proteinases, or changes in environment such as pH) [69,70]; and (4) labeled cells, by which agents can be bound to or introduced into specific cell types e.g. stem cells or T-cells, which then rely on the trafficking and recognition of the cells for their localization [71,72].

Just as the sensitivity for detecting the presence of radionuclei depends on the target to background ratio (≈ the effective SNR), our ability to detect changes in relaxation times also depends on the magnitude of the effect of the agent compared with a background relaxation rate; that is, the magnitude of changes due to the agent must be significantly different from the intrinsic relaxation rate within tissues. An upper limit on relaxation times is given by pure water, in which dipole–dipole interactions between protons shorten T1 to approximately 4 s. For most soft tissues at clinical imaging fields, the longitudinal relaxation rate R_1 ($=1/T_1$) is higher, of order 1 sec^{-1}. Given the intrinsic variations of relaxation rates within a tissue (a few percent) and the available SNR of typical images, it is reasonable to stipulate the minimum detectable change in background relaxation rate to be on the order of 10%; that is, we require the minimum change in rate caused by an agent, ΔR_{1min}, to be approximately 0.10 sec^{-1}. The efficacy of relaxation agents in MRI is usually described in terms of the relaxivity, or the change in R_1 per unit concentration of agent. The most common agents in use, such as gadolinium-DTPA, have relaxivities of approximately 4 $sec^{-1}mM^{-1}$ (slightly more or less at lower or higher field strengths, respectively), but in principle the relaxivity of some paramagnetic agents may be enhanced by, for example, binding to a macromolecule (for a discussion of the factors affecting MRI contrast agents, see e.g. Gore et al. [73]). If the enhancement factor relative to gadolinium- DTPA is ε, then the relaxivity of the agent is 4ε $sec^{-1}mM^{-1}$; setting the minimum value of ΔR_1 equal to 0.10 sec^{-1}, the necessary concentration for detection is $25/\varepsilon$ μM.

The Solomon–Bloembergen–Morgan equations [73] describe how relaxivity varies with factors such as the magnetic field, the correlation times of the local fluctuating magnetic fields produced by the agent that promote relaxation, and the distance between the paramagnetic species and the relaxing nuclei; in theory, enhancements of roughly two orders of magnitude may be possible. To date, however, these have not been achieved, and in

practice only more modest gains may be possible in vivo. Thus, if a reasonable achievable value for ε is taken to be 25, our required concentration of metal (gadolinium) is 1 μM. This is the necessary concentration averaged over the voxel if it is to "stand out" as having an MR signal 10% above the background, and corresponds to only a picoMole within a voxel of 1×1×1 mm. However, this is still much higher than the levels detected in, for example, nuclear imaging methods such as PET. For small-molecule targeting with one or a few metal ions per molecule, the number of ligand sites or receptors in each and every cell that bind the agent would have to be very high (of order 10^{11} to 10^{12}) to achieve this average level of metal in the tissue voxel. However, as an alternative approach, these atoms might be delivered within a single particle or package such as a liposome, or attached in large quantities to a dendrimer or biopolymer. The relaxation effects of the paramagnetic payload may then be spread to affect all other water within the voxel as long as the water is free to exchange in and out of the vicinity of the metal ions in the time scale available. For example, if a suitable particle contains a solution of the contrast agent that has concentration 1 M, then to achieve a voxel concentration of 1 μM requires the particle size be such that it occupies 10^{-6} of the voxel volume, or has dimension 10^{-2} of the voxel dimension e.g. if the voxel is 1 mm^3 in size the particle has to be 10 μm to produce the required contrast (i.e., a concentration of 1 μM of gadolinium). The single particle may be substituted by a larger number of smaller particles e.g. 1000 particles of size 1 μm in 1 mm^3 voxel. The important quantity is the average concentration of metal within the voxel; if the agent is highly localized, then it may be advantageous to acquire images with higher spatial resolution to minimize dilution of the effect by partial-volume averaging.

An alternative to T_1-reducing paramagnetic agents is provided by so-called susceptibility agents, such as superparamagnetic iron oxide particles [74]. These reduce tissue transverse relaxation rates by altering the magnetic field in their vicinity, thereby inducing signal dephasing within the nonuniform field, and their effects extend over distances that depend on their size and other factors. The relaxivity per iron atom can be quite high, equivalent to obtaining an enhancement factor for transverse effects >100. However, the background relaxation rate that must be altered is also much higher than R_1—typically, R_2* is about 20 × R_1. Thus, instead of a change in R_1 of 0.1 we seek to achieve a change in R_2* of 2. Roughly, therefore, the relative efficacy of R_2* agents versus R_1 agents would be 5 times greater than particles containing 1 M gadolinium for the same molarity of metal. We recently reported [98] estimates of the numbers of particles of iron oxide of different sizes that would be required to achieve significant effects. For larger (≈ micron sized) particles, it should be possible to detect a single particle in a small voxel, and such effects have been reported by several groups.

An alternative class of contrast agents has been developed which exploit magnetization transfer effects between water molecules in the tissue and protons in the exogenous agent. The latter protons have a different resonance frequency (a chemical shift) to water and undergo chemical exchange at tissue pH. Contrast effects are produced by applying radiofrequency pulses at the resonance frequency of these labile protons which changes their magnetization (they become completely or partially saturated). This saturation is then communicated to the water protons by magnetization transfer as the nuclei undergo exchange, so that the larger bulk water signal is decreased, thereby reporting the presence of the labile species. This is the basis of CEST (chemical exchange saturation transfer) and PARACEST (paramagnetic chemical exchange saturation transfer) agents (which incorporate a paramagnetic center to shift the resonance frequencies farther apart) [75, 76]. The signal change depends on the rate of exchange between the different species, which must be fast enough to produce large effects. CEST contrast may be quite sensitive to physicochemical factors such as pH. However, even under the most favorable circumstances

currently projected, the molar concentration of agent within a voxel required for detection is still required to be large relative to the concentrations detected in nuclear imaging.

It may be concluded from the above that specific targeting using small molecules is highly unlikely to achieve high enough levels of agent to produce measurable changes in MR signals. On the other hand, the detection of large targeted particles (≈ 0.1 – 1 micron) containing high concentrations of metal (Gd or Fe or a PARACEST agent) may be feasible at high spatial resolution, and much work continues in this area especially as new concepts evolve from developments in nanomaterials. However, there other intriguing approaches that do not rely on being able to achieve specific spatial distributions of an agent such that the requirement of targeting of molecular imaging agents can be relaxed. This potential arises from the unique feature of MR contrast agents that their efficacy can be modified by the physico-chemical environment [73]. Radionuclear methods are very sensitive but the information they provide is contained *only* in the spatial distribution and kinetics of carrier molecules. The gamma emission from PET agents is barely affected by the environment in which the positron annihilates. This is not true for MRI agents such as T_1-reducing paramagnetic materials, which can change their relaxation efficacy because of changes in the local environment. For example, manganese and gadolinium ions are both effective paramagnetic contrast agents, but their relaxivities may increase markedly when they are bound to large molecules so that they tumble more slowly, and they may decrease when they are contained in a cage that restricts water access [73]. Similarly, CEST and PARACEST agents can be developed in which the number and rate of exchange of labile protons is altered by an environmental factor such as pH or the presence of specific ligands [77]. This has given rise to the development of “smart agents” in which the characteristics of the probe e.g. relaxivity vary with the environment and may report on cellular and molecular processes without the need for specific targeting. For example, the agent may distribute in non-specific manner but the relaxivity may change only where specific enzymes are abundant that appropriately modify the structure. An early example of this [78] showed how a Gd based agent could increase its effect as a paramagnetic relaxation agent only when the carrier molecule was cleaved by a specific enzyme which thereby allowed water to access the Gd ion and feel its effect on relaxation. SImilar smart agents have been developed that sense pH, or specific solutes such as glucose [79, 80]. Thus, even if the targeting of the agent is non-specific, the effects in MR images may be locally specific. Of course, the concentration of the agent in the voxel must still be large enough to produce detectable effects, but the design of the agent has different constraints when the targeting requirement is relaxed.

Magnetic Resonance Spectral Imaging

Nuclear imaging detects the emissions from radioactive decays but cannot distinguish between atoms in different molecules and thus is not sensitive to chemical changes. Conversely, high resolution NMR spectra in which distinct chemical species are separately identifiable by their resonance frequencies provide true chemical specificity. High resolution spectra can be obtained from single, isolated volumes or, by combining spatial encoding with spectral analysis, separate images of each spectral component can be acquired. Spectral or chemical shift imaging (CSI) arguably fits the definition of molecular imaging better than any other modality because the measured quantities actually change with molecular chemistry. CSI has long been used at low spectral resolution for providing fat and water images separately [81], and the signal to noise ratios of these images is relatively high because water and lipids occur in high abundance in tissues of interest. As mentioned earlier, lower level metabolites of millimolar concentrations may also be mapped at the resolution (≈ 1mL) of nuclear images in reasonable times (several minutes) e.g. maps of major brain metabolites N-acetyl aspartate, creatine and choline. Phosphorus-31 metabolites such as ATP and PCr may be spatially mapped in similar manner, albeit with lower

sensitivity and spatial resolution [82]. As mentioned earlier, direct detection of labelled substrates can also be achieved, and there is particular value in recording high resolution spectra from volumes of tissue in which ^{13}C-labelled compounds are metabolized. For example, glucose labelled with ^{13}C can be infused and the subsequent appearance of the labelled carbon in other parts of the spectrum can be used to detect metabolic conversion of the glucose into other compounds [83]. For example, in the brain it is possible over time to follow the carbon label into the molecular structures of glutamate and glutamine, and from those spectra to infer rates of conversion [84]. Note that the amounts required are still quite high, and this is one of the incentives for developing hyperpolarization techniques described below.

Less specific information of a chemical nature can also be obtained using the principles of CEST imaging described earlier, but in which the labile protons that cause signal changes upon saturation arise from endogenous species such as the amide protons found mainly in naturally abundant amino acids, peptides and proteins, or the hydroxyl protons present in e.g. glucose and glycogen [85, 86]. Two variants of CEST termed amide proton transfer (APT) [85] and glycoCEST [86] have been developed to enable specific observations of the magnetization transfer effects on water following saturation of the amides and hydroxyl protons respectively, and have been used to infer molecular changes associated with tumor composition and muscle and liver metabolism. These methods have intrinsically higher signal to noise because the effects of low levels of metabolites are amplified by their effects on the much larger water signals, but their interpretation depends on how specifically the exchanging species can be associated with particular constituents of tissues.

Hyperpolarized MRI

NMR is inherently a relatively insensitive type of spectroscopy because only a small fraction of the nuclei in the sample actually contribute to measured signals. The equilibrium magnetization induced in a sample in a magnetic field depends on the strength of the interaction between individual nuclei and the field. Normally, for spin 1/2 nuclei such as ^{1}H and ^{13}C, in thermal equilibrium the nuclei distribute themselves among the two allowed energy levels (corresponding to alignment or opposition to the field) almost evenly, with a small minority (typically about 5 in a million at 3 Tesla) predicted by the Boltzman distribution of energy states. However, for special cases and specific nuclei, a large increase in magnetization and thus MR signal can be achieved using hyperpolarization, by which the equilibrium Boltzman distribution is disturbed to achieve a much less even distribution of energy levels and, consequently, a larger magnetization. The hyperpolarization must take place out of the body by exposing appropriate substrates to some kind of spin-exchange mechanism, after which they may be introduced into the subject for imaging. This has been successfully achieved for the gases 3He and 129Xe [87, 88], and more recently for molecules containing ^{13}C or ^{15}N [89, 90], allowing the exciting possibility of imaging metabolic pathways. Hyperpolarization reduces the minimum required concentration by several orders of magnitude, allowing, for example, exquisite portrayal of the lungs using direct imaging of helium in the airways at a resolution and SNR comparable to conventional proton imaging of water [87]. Further work is needed, however, to establish the practical role of hyperpolarized labeled metabolites, especially given that in vivo the lifetime of the magnetization is usually quite limited (tens of seconds or less in many cases) and there may not be enough time for molecules to access sites of interest and be sufficiently involved in biochemical processes to provide adequate sensitivity. However, preliminary images have been produced depicting the uptake and turnover of metabolic substrates.

Much of the effort in hyperpolarized imaging in cancer has been focused on direct and indirect assays of pyruvate metabolism. Relative to normal cells, a disproportionate conversion of pyruvate to lactate is commonly observed in tumors, and flux through this

pathway appears to provide information analogous to glucose uptake determined from FDG-PET [91]. While the in vivo flux through lactate dehydrogenase has been most fruitful and abundant, citric acid cycle conversion (fumarate to malate) and pH have also been measured with hyperpolarized MR *in vivo*. Patterns in hyperpolarized pyruvate conversion are conspicuous in vivo and appear to provide unambiguous differentiation from surrounding tissue. Chemical shift images with an effective resolution of (2.5×2.5×10) mm^3 collected 30 s after infusion of 79 mM hyperpolarized sodium $^{13}C_1$-pyruvate were acquired across a region encompassing skeletal muscle, P22 tumor implant and vena cava. $^{13}C_1$-pyruvate was observed in all three regions while $^{13}C_1$-lactate was elevated only in tumor tissue. It is not generally possible to discern tissue conversion versus conversion and subsequent transport, but this concern is diminished considering that low lactate production appeared in anatomies with high blood volume [92].

The used of hyperpolarized pyruvate has also recently been extended to assessing tumor grade and response to therapy [93]. Histopathology of resected transgenic adenocarcinomas of mouse prostate tumors (TRAMP) demonstrated that $^{13}C_1$-lactate produced from infused $^{13}C_1$-pyruvate was a sensitive and specific biomarker for tumor grade. To assess lactate time-courses, a 79 mM $^{13}C_1$-pyruvate solution at pH 7.9 was infused over 12 s, and 10 mm slabs positioned on the primary tumor were collected at 3 s temporal resolution using 5 degree excitation pulses. Subsequent MRSI data were acquired with 0.135 cm^3 spatial resolution at the $^{13}C_1$-lactate plateau which was estimated to occur between 35 and 49 ms post-infusion [93].

In addition to showing promise in detecting and grading tumors, hyperpolarized $^{13}C_1$-pyruvate imaging and spectroscopy have also been used to detect response to therapy. Day and coworkers [94] measured the production of lactate from a 75 mM $^{13}C_1$-pyruvate solution in subcutaneously implanted EL-4 cells and found that flux through lactate dehydrogenase was decreased within 24 hours of therapy. In this study, spectroscopic (pulse-acquire) data were collected over 160 s with 5 degree flip angles and ^{13}C chemical shift images were acquired with a 32×32 mm field of view and 16×16 data matrix [94].

As a correlate of abnormal metabolism, tumors are often more acidic than normal tissue. The balance of $^{13}C0_2$ and $H^{13}C0_3^-$ reflects *in vivo* pH and therefore this reaction equilibrium can potentially be used to distinguish cancerous tissue. The ratio of these compounds has been measured *in vivo* in mice with subcutaneous lymphomas by Gallagher et al. and shown to identify tumor tissue when overlaid on anatomical images. In these experiments, carbon-13 images were acquired 10 s after infusion of hyperpolarized 100 mM bicarbonate with a 16×16 matrix and 2×2×6 mm voxels [95].

The detection of abnormal metabolism in tumors by hyperpolarized MR is not limited to imaging glycolytic surrogates. The production of [1, 4-^{13}C]malate from [1, 4-^{13}C]fumarate has been used to assess tumor necrosis and treatment response in murine lymphoma tumors [96]. ^{13}C chemical shift images acquired 30 s after fumarate infusion showed that malate was concentrated in tumors relative to its precursor and a large increase in [1, 4-^{13}C]malate was correlated to treatment. Chemical shift images were acquired in 5 s with a 35×35 mm field of view and 16×16 data matrix [96].

Others have proposed the imaging of ^{15}N-hyperpolarized choline as a biomarker of elevated choline metabolism in human cancer [97]. ^{15}N-hyperpolarized choline is currently known to be the longest lived hyperpolarized metabolic contrast agent i*n vivo* with $T_1 \approx 126$ s, corresponding to a half life $t_{1/2} = 89$ s. This agent has a short lifetime compared to the F18 isotope, but it appears this time scale is sufficient to observe metabolic events of tissue

uptake and phosphorylation. At the time of this review this approach to molecular imaging for quantifying the spatial distributions of metabolic fluxes appears promising.

Summary

MRI continues to make remarkable progress in many different directions Robust imaging biomarkers e.g. ADC and DCE-derived parameters, can give insight into important biophysical, physiological and metabolic properties of tissues, and will be important adjuncts to other cellular and molecular imaging methods. Such measurements are likely to be of broad use in patient stratification, for selecting treatments, and for assessing treatment response in individual subjects. Targeted, specific molecular imaging probes of the sort that are used as PET and SPECT imaging agents are unlikely to enjoy widespread success with MRI, though there are several possible strategies for achieving the high concentrations of contrast agent needed in the tissues of interest [98]. MRI however also provides unique opportunities for smart contrast agents, and for hyperpolarized imaging. MRS is also a unique molecular imaging modality in its ability to provide chemically specific information and changes in molecular structures. Even after 30 years of progress there are still many exciting new directions for advancement and creative ideas on how to incorporate new MR methods into medical practice and research in the era of molecular imaging.

Acknowledgments

We gratefully acknowledge the following grant support from the National Institutes of Health: CA109106, CA128323, EB000214 (awarded to JCG), CA140628, CA127349, CA145138 (awarded to HCM), CA127599 (awarded to CCQ) and CA142565, CA138599, CA129961 (awarded to TEY)

References

1. Pruessmann KP, Weiger M, Scheidegger MB, Boesiger P. SENSE: sensitivity encoding for fast MRI. Magn Reson Med. 1999; 42:952–62. [PubMed: 10542355]
2. Lustig M, Donoho D, Pauly JM. Sparse MRI: The application of compressed sensing for rapid MR imaging. Magn Reson Med. 2007; 58:1182–95. [PubMed: 17969013]
3. Robitaille PM, Abduljalil AM, Kangarlu A. Ultra high resolution imaging of the human head at 8 tesla: 2K × 2K for Y2K. J Comput Assist Tomogr. 2000; 24:2–8. [PubMed: 10667650]
4. Molecular Imaging Center of Excellence, Society of Nuclear Medicine. see http://www.molecularimagingcenter.org
5. Atkinson AJ Jr, Colburn WA, DeGruttola VG, DeMets DL, Downing GJ, Hoth DF, Oates JA, Peck CC, Schooley RT, Spilker BA, Woodcock JW, Zeger SL. Biomarkers and surrogate endpoints: Preferred definitions and conceptual framework. Clin Pharmacol Ther. 2001; 69:89–95. [PubMed: 11240971]
6. Therasse P, Arbuck SG, Eisenhauer EA, Wanders J, Kaplan RS, Rubinstein L, Verweij J, Van Glabbeke M, van Oosterom AT, Christian MC, Gwyther SG. New guidelines to evaluate the response to treatment in solid tumors. J Natl Cancer Inst. 2000; 92:205–16. [PubMed: 10655437]
7. Zhong JH, Gore JC. Studies of restricted diffusion in heterogeneous media containing variations in susceptibility. Magn Reson Med. 1991; 19:276–84. [PubMed: 1881316]
8. Anderson AW, Zhong J, Petroff OAC, Szafer A, Ransom BR, Prichard JW, Gore JC. Effects of osmotically-driven cell volume changes on diffusion weighted imaging of the rat optic nerve. Magn Reson Med. 1995; 35:162–167. [PubMed: 8622579]
9. Sugahara T, Korogi Y, Kochi M, Ikushima I, Shigematu Y, Hirai T, Okuda T, Liang LX, Ge YL, Komohara Y, Ushio Y, Takahashi M. Usefulness of diffusion-weighted MRI with echo-planar technique in the evaluation of cellularity in gliomas. Journal of Magnetic Resonance Imaging. 1999; 9:53–60. [PubMed: 10030650]

10. Lyng H, Haraldseth O, Rofstad EK. Measurement of cell density and necrotic fraction in human melanoma xenografts by diffusion weighted magnetic resonance imaging. Magnetic Resonance in Medicine. 2000; 43:828–836. [PubMed: 10861877]
11. Tsuruda JS, Chew WM, Moseley ME, Norman D. Diffusion-weighted MR imaging of extraaxial tumors. Magn Reson Med. 1991; 19:316–20. [PubMed: 1881321]
12. Maeda M, Kawamura Y, Tamagawa Y, Matsuda T, Itoh S, Kimura H, Iwasaki T, Hayashi N, Yamamoto K, Ishii Y. Intravoxel incoherent motion (IVIM) MRI in intracranial, extraaxial tumors and cysts. J Comput Assist Tomogr. 1992; 16:514–8. [PubMed: 1629406]
13. Tien RD, Felsberg GJ, Friedman H, Brown M, MacFall J. MR imaging of high-grade cerebral gliomas: value of diffusion-weighted echoplanar pulse sequences. AJR Am J Roentgenol. 1994; 162:671–7. [PubMed: 8109520]
14. Brunberg JA, Chenevert TL, McKeever PE, Ross DA, Junck LR, Muraszko KM, Dauser R, Pipe JG, Betley AT. In vivo MR determination of water diffusion coefficients and diffusion anisotropy: correlation with structural alteration in gliomas of the cerebral hemispheres. AJNR Am J Neuroradiol. 1995; 16:361–71. [PubMed: 7726086]
15. Eis M, Els T, Hoehn-Berlage M. High resolution quantitative relaxation and diffusion MRI of three different experimental brain tumors in rat. Magn Reson Med. 1995; 34:835–44. [PubMed: 8598810]
16. Zhao M, Pipe JG, Bonnett J, Evelhoch JL. Early detection of treatment response by diffusion-weighted 1H-NMR spectroscopy in a murine tumour in vivo. Br J Cancer. 1996; 73:61–4. [PubMed: 8554985]
17. Chenevert TL, McKeever PE, Ross BD. Monitoring early response of experimental brain tumors to therapy using diffusion magnetic resonance imaging. Clinical Cancer Research. 1997; 3:1457–1466. [PubMed: 9815831]
18. Chenevert TL, Stegman LD, Taylor JMG, Robertson PL, Greenberg HS, Rehemtulla A, Ross BD. Diffusion magnetic resonance imaging: an early surrogate marker of therapeutic efficacy in brain tumors. Journal of the National Cancer Institute. 2000; 92:2029–2036. [PubMed: 11121466]
19. Hakumaki JM, Poptani H, Puumalainen AM, Loimas S, Paljarvi LA, Yla-Herttuala S, Kauppinen RA. Quantitative H-1 nuclear magnetic resonance diffusion spectroscopy of BT4C rat glioma during thymidine kinase- mediated gene therapy in vivo: Identification of apoptotic response. Cancer Research. 1998; 58:3791–3799. [PubMed: 9731486]
20. Poptani H, Puumalainen AM, Grohn OH, Loimas S, Kainulainen R, Yla-Herttuala S, Kauppinen RA. Monitoring thymidine kinase and ganciclovir-induced changes in rat malignant glioma in vivo by nuclear magnetic resonance imaging. Cancer Gene Therapy. 1998; 5:101–109. [PubMed: 9570301]
21. Galons JP, Altbach MI, Paine-Murrieta GD, Taylor CW, Gillies RJ. Early increases in breast tumor xenograft water mobility in response to paclitaxel therapy detected by non-invasive diffusion magnetic resonance imaging. Neoplasia. 1999; 1:113–7. [PubMed: 10933044]
22. Stegman LD, Rehemtulla A, Hamstra DA, Rice DJ, Jonas SJ, Stout KL, Chenevert TL, Ross BD. Diffusion MRI detects early events in the response of a glioma model to the yeast cytosine deaminase gene therapy strategy. Gene Therapy. 2000; 7:1005–1010. [PubMed: 10871748]
23. Guo AC, Cummings TJ, Dash RC, Provenzale JM. Lymphomas and high-grade astrocytomas: comparison of water diffusibility and histologic characteristics. Radiology. 2002; 224:177–83. [PubMed: 12091680]
24. Kauppinen RA. Monitoring cytotoxic tumour treatment response by diffusion magnetic resonance imaging and proton spectroscopy. Nmr in Biomedicine. 2002; 15:6–17. [PubMed: 11840548]
25. Brauer M. In vivo monitoring of apoptosis. Progress in Neuro-Psychopharmacology & Biological Psychiatry. 2003; 27:323–331. [PubMed: 12657370]
26. Dzik-Jurasz A, Domenig C, George M, Wolber J, Padhani A, Brown G, Doran S. Diffusion MRI for prediction of response of rectal cancer to chemoradiation. Lancet. 2002; 360(9329):307–8. [PubMed: 12147376]
27. Koh DM, Scurr E, Collins D, Kanber B, Norman A, Leach MO, Husband JE. Predicting response of colorectal hepatic metastasis: value of pretreatment apparent diffusion coefficients. AJR Am J Roentgenol. 2007; 188:1001–8. [PubMed: 17377036]

28. Cui Y, Zhang XP, Sun YS, Tang L, Shen L. Apparent diffusion coefficient: potential imaging biomarker for prediction and early detection of response to chemotherapy in hepatic metastases. Radiology. 2008; 248:894–900. [PubMed: 18710982]
29. Moffat BA, Chenevert TL, Lawrence TS, Meyer CR, Johnson TD, Dong Q, Tsien C, Mukherji S, Quint DJ, Gebarski SS, Robertson PL, Junck LR, Rehemtulla A, Ross BD. Functional diffusion map: a noninvasive MRI biomarker for early stratification of clinical brain tumor response. Proc Natl Acad Sci U S A. 2005; 102:5524–9. [PubMed: 15805192]
30. Hall DE, Moffat BA, Stojanovska J, Johnson TD, Li Z, Hamstra DA, Rehemtulla A, Chenevert TL, Carter J, Pietronigro D, Ross BD. Therapeutic efficacy of DTI-015 using diffusion magnetic resonance imaging as an early surrogate marker. Clin Cancer Res. 2004; 10(23):7852–9. [PubMed: 15585617]
31. Lee KC, Sud S, Meyer CR, Moffat BA, Chenevert TL, Rehemtulla A, Pienta KJ, Ross BD. An imaging biomarker of early treatment response in prostate cancer that has metastasized to the bone. Cancer Res. 2007; 67(8):3524–8. [PubMed: 17440058]
32. Yankeelov TE, Lepage M, Chakravarthy A, Broome EE, Niermann KJ, Kelley MC, Meszoely I, Mayer IA, Herman CR, McManus K, Price RR, Gore JC. Integration of quantitative DCE-MRI and ADC mapping to monitor treatment response in human breast cancer: initial results. Magn Reson Imaging. 2007; 25:1–13. [PubMed: 17222711]
33. Morse DL, Galons JP, Payne CM, Jennings DL, Day S, Xia G, Gillies RJ. MRI-measured water mobility increases in response to chemotherapy via multiple cell-death mechanisms. NMR Biomed. 2007; 20(6):602–14. [PubMed: 17265424]
34. Kim H, Morgan DE, Zeng H, Grizzle WE, Warram JM, Stockard CR, Wang D, Zinn KR. Breast tumor xenografts: diffusion-weighted MR imaging to assess early therapy with novel apoptosis-inducing anti-DR5 antibody. Radiology. 2008; 248(3):844–51. [PubMed: 18710978]
35. Seierstad T, Røe K, Olsen DR. Noninvasive monitoring of radiation-induced treatment response using proton magnetic resonance spectroscopy and diffusion-weighted magnetic resonance imaging in a colorectal tumor model. Radiother Oncol. 2007; 85(2):187–94. [PubMed: 17937968]
36. Folkman J. Angiogenesis in cancer, vascular, rheumatoid and other disease. Nat Med. 1995; 1:27–31. [PubMed: 7584949]
37. Yankeelov TE, Gore JC. Dynamic contrast enhanced magnetic resonance imaging in oncology: Theory, data acquisition, analysis, and examples. Current Medical Imaging Reviews. 2007; 3:91–107. [PubMed: 19829742]
38. Li K-L, Wilmes LJ, Henry RG, Pallavicini MG, Park JW, Hu-Lowe DD, McShane TM, Shalinsky DR, Fu Y-J, Brasch RC, Hylton NM. Heterogeneity in the angiogenic response of a BT474 human breast cancer to a novel vascular endothelial growth factor-receptor tyrosine kinase inhibitor: Assessment by voxel analysis of dynamic contrast-enhanced MRI. J Magn Reson Imaging. 2005; 22:511–9. [PubMed: 16161072]
39. Ellingsen C, Egeland TA, Gulliksrud K, Gaustad JV, Mathiesen B, Rofstad EK. Assessment of hypoxia in human cervical carcinoma xenografts by dynamic contrast-enhanced magnetic resonance imaging. Int J Radiat Oncol Biol Phys. 2009; 73:838–45. [PubMed: 19215820]
40. Dafni H, Kim SJ, Bankson JA, Sankaranarayanapillai M, Ronen SM. Macromolecular dynamic contrast-enhanced (DCE)-MRI detects reduced vascular permeability in a prostate cancer bone metastasis model following anti-platelet-derived growth factor receptor (PDGFR) therapy, indicating a drop in vascular endothelial growth factor receptor (VEGFR) activation. Magn Reson Med. 2008; 60:822–33. [PubMed: 18816866]
41. Moasser MM, Wilmes LJ, Wong CH, Aliu S, Li KL, Wang D, Hom YK, Hann B, Hylton NM. Improved tumor vascular function following high-dose epidermal growth factor receptor tyrosine kinase inhibitor therapy. J Magn Reson Imaging. 2007; 26:1618–25. [PubMed: 17968965]
42. Muruganandham M, Lupu M, Dyke JP, Matei C, Linn M, Packman K, Kolinsky K, Higgins B, Koutcher JA. Preclinical evaluation of tumor microvascular response to a novel antiangiogenic/antitumor agent RO0281501 by dynamic contrast-enhanced MRI at 1.5 T. Mol Cancer Ther. 2006; 5:1950–7. [PubMed: 16928815]
43. Marzola P, Degrassi A, Calderan L, Farace P, Nicolato E, Crescimanno C, Sandri M, Giusti A, Pesenti E, Terron A, Sbarbati A, Osculati F. Early antiangiogenic activity of SU11248 evaluated in

vivo by dynamic contrast-enhanced magnetic resonance imaging in an experimental model of colon carcinoma. Clin Cancer Res. 2005; 11:5827–32. [PubMed: 16115922]

44. Ah-See M-LW, Makris A, Taylor NJ, Harrison M, Richman PI, Burcombe RJ, Stirling JJ, d'Arcy JA, Collins DJ, Pittam MR, Ravichandran D, Padhani AR. Early Changes in Functional Dynamic Magnetic Resonance Imaging Predict for Pathologic Response to Neoadjuvant Chemotherapy in Primary Breast Cancer. Clin Cancer Res. 2008; 14:6580–9. [PubMed: 18927299]
45. Hahn OM, Yang C, Medved M, Karczmar G, Kistner E, Karrison T, Manchen E, Mitchell M, Ratain MJ, Stadler WM. Dynamic contrast-enhanced magnetic resonance imaging pharmacodynamic biomarker study of sorafenib in metastatic renal carcinoma. J Clin Oncol. 2008; 26:4572–8. [PubMed: 18824708]
46. Li KL, Henry RG, Wilmes LJ, Gibbs J, Zhu X, Lu Y, Hylton NM. Kinetic assessment of breast tumors using high spatial resolution signal enhancement ratio (SER) imaging. Magn Reson Med. 2007; 58:572–81. [PubMed: 17685424]
47. Oberholzer K, Pohlmann A, Schreiber W, Mildenberger P, Kunz P, Schmidberger H, Junginger T, Düber C. Assessment of tumor microcirculation with dynamic contrast-enhanced MRI in patients with esophageal cancer: initial experience. J Magn Reson Imaging. 2008; 27:1296–301. [PubMed: 18504749]
48. Radjenovic A, Dall BJ, Ridgway JP, Smith MA. Measurement of pharmacokinetic parameters in histologically graded invasive breast tumours using dynamic contrast-enhanced MRI. Br J Radiol. 2008; 81:120–8. [PubMed: 18070824]
49. Haider MA, Sitartchouk I, Roberts TP, Fyles A, Hashmi AT, Milosevic M. Correlations between dynamic contrast-enhanced magnetic resonance imaging-derived measures of tumor microvasculature and interstitial fluid pressure in patients with cervical cancer. J Magn Reson Imaging. 2007; 25:153–9. [PubMed: 17173303]
50. Kennan RP, Zhong J, Gore JC. Intravascular susceptibility contrast mechanisms in tissues. Magn Reson Med. 1994; 31:9–21. [PubMed: 8121277]
51. Aronen HJ, Gazit IE, Louis DN, Buchbinder BR, Pardo FS, Weisskoff RM, Harsh GR, Cosgrove GR, Halpern EF, Hochberg FH. Cerebral blood volume maps of gliomas: comparison with tumor grade and histologic findings. Radiology. 1994; 191(1):41–51. [PubMed: 8134596]
52. Donahue KM, Krouwer HG, Rand SD, Pathak AP, Marszalkowski CS, Censky SC, Prost RW. Utility of simultaneously acquired gradient-echo and spin-echo cerebral blood volume and morphology maps in brain tumor patients. Magnetic Resonance in Medicine. 2000; 43(6):845–853. [PubMed: 10861879]
53. Schmainda KM, Rand SD, Joseph AM, Lund R, Ward BD, Pathak AP, Ulmer JL, Badruddoja MA, Krouwer HG. Characterization of a first-pass gradient-echo spin-echo method to predict brain tumor grade and angiogenesis. AJNR Am J Neuroradiol. 2004; 25(9):1524–1532. [PubMed: 15502131]
54. Hakyemez B, Erdogan C, Ercan I, Ergin N, Uysal S, Atahan S. High-grade and low-grade gliomas: differentiation by using perfusion MR imaging. Clin Radiol. 2005; 60(4):493–502. [PubMed: 15767107]
55. Fuss M, Wenz F, Essig M, Muenter M, Debus J, Herman TS, Wannenmacher M. Tumor angiogenesis of low-grade astrocytomas measured by dynamic susceptibility contrast-enhanced MRI (DSC-MRI) is predictive of local tumor control after radiation therapy. International Journal of Radiation Oncology, Biology, Physics. 2001; 51(2):478–482.
56. Weber MA, Thilmann C, Lichy MP, Gunther M, Delorme S, Zuna I, Bongers A, Schad LR, Debus J, Kauczor HU, Essig M, Schlemmer HP. Assessment of irradiated brain metastases by means of arterial spin-labeling and dynamic susceptibility-weighted contrast-enhanced perfusion MRI: initial results. Invest Radiol. 2004; 39(5):277–287. [PubMed: 15087722]
57. Lee MC, Cha S, Chang SM, Nelson SJ. Dynamic susceptibility contrast perfusion imaging of radiation effects in normal-appearing brain tissue: changes in the first-pass and recirculation phases. J Magn Reson Imaging. 2005; 21(6):683–693. [PubMed: 15906330]
58. Delile J, Slanetz P, Yeh E, Kopans D, Garrido L. Breast Cancer: Regional blood flow and volume with magnetic susceptibility-based MR imaging. Radiology. 2002; 223:558–565. [PubMed: 11997568]

59. Ludemann L, Prochnow D, Rohlfing T, Franiel T, Warmuth C, Taupitz M, Rehbein H, Beyersdorff D. Simultaneous quantification of perfusion and permeability in the prostate using dynamic contrast-enhanced magnetic resonance imaging with an inversion-prepared dual-contrast sequence. Ann Biomed Eng. 2009; 37(4):749–762. [PubMed: 19169821]
60. Tropes I, Grimault S, Vaeth A, Grillon E, Julien C, Payen J-F, Lamalle L, Decorps M. Vessel Size Imaging. Magnetic Resonance in Medicine. 2001; 45:397–408. [PubMed: 11241696]
61. Quarles CC, Gochberg DF, Gore JC, Yankeelov TE. A theoretical framework to model DSC-MRI data acquired in the presence of contrast agent extravasation. Phys Med Biol. 2009; 54(19):5749–5766. [PubMed: 19729712]
62. Kreis R. Quantitative localized 1H MR spectroscopy for clinical use. Progress in Nuclear Magnetic Resonance Spectroscopy. 1997; 31:155–195.
63. Osorio JA, Ozturk-Isik E, Xu D, Cha S, Chang S, Berger MS, Vigneron DB, Nelson SJ. 3D 1H MRSI of brain tumors at 3.0 Tesla using an eight-channel phased-array head coil. J Magn Reson Imaging. 2007; 26:23–30. [PubMed: 17659562]
64. Sherry AD, Woods M. Chemical Exchange Saturation Transfer Contrast Agents for Magnetic Resonance Imaging. Annu Rev Biomed Eng. 2008; 10:391–411. [PubMed: 18647117]
65. Bellin MF, Vasile M, Morel-Precetti S. Currently used non-specific extracellular MR contrast media. Eur Radiol. 2003; 13:2688–98. [PubMed: 12819914]
66. Mohs AM, Lu ZR. Gadolinium(III)-based blood-pool contrast agents for magnetic resonance imaging: status and clinical potential. Expert Opin Drug Deliv. 2007; 4:149–64. [PubMed: 17335412]
67. Artemov D. Molecular magnetic resonance imaging with targeted contrast agents. J Cell Biochem. 2003; 90:518–24. [PubMed: 14523986]
68. Krishnan AS, Neves AA, de Backer MM, Hu DE, Davletov B, Kettunen MI, Brindle KM. Detection of cell death in tumors by using MR imaging and a gadolinium-based targeted contrast agent. Radiology. 2008; 246(3):854–62. [PubMed: 18187402]
69. Lepage M, Dow WC, Melchior M, You Y, Fingleton B, Quarles CC, Pépin C, Gore JC, Matrisian LM, McIntyre JO. Noninvasive detection of matrix metalloproteinase activity in vivo using a novel magnetic resonance imaging contrast agent with a solubility switch. Mol Imaging. 2007; 6:393–403. [PubMed: 18053410]
70. Yoo B, Pagel MD. An overview of responsive MRI contrast agents for molecular imaging. Front Biosci. 2008; 13:1733–52. [PubMed: 17981664]
71. Rogers WJ, Meyer CH, Kramer CM. Technology insight: in vivo cell tracking by use of MRI. Nat Clin Pract Cardiovasc Med. 2006; 3:554–62. [PubMed: 16990841]
72. Bulte JW, Duncan ID, Frank JA. In vivo magnetic resonance tracking of magnetically labeled cells after transplantation. J Cereb Blood Flow Metab. 2002; 22:899–907. [PubMed: 12172375]
73. Gore, JC.; Joers, JM.; Kennan, RP. Contrast Agents and Relaxation Effects. In: Atlas, Scott, editor. Magnetic Resonance Imaging of the Brain and Spine. 3. Vol. Chapter 4. Lippincott: Williams and Wilkins; 2002. p. 79-99.
74. Majumdar S, Zoghbi SS, Pope CF, Gore JC. A quantitative study of relaxation rate enhancement produced by iron-oxide particles in polyacrylamide gels and tissue. Mag Res Med. 1989; 9:185–202.
75. Zhang S, Merritt M, Woessner DE, Lenkinski RE, Sherry AD. PARACEST agents: modulating MRI contrast via water proton exchange. Acc Chem Res. 2003; 36:783–90. [PubMed: 14567712]
76. Woods M, Woessner DE, Sherry AD. Paramagnetic lanthanide complexes as PARACEST agents for medical imaging. Chem Soc Rev. 2006; 5(6):500–11. [PubMed: 16729144]
77. Ren J, Trokowski R, Zhang S, Malloy CR, Sherry AD. Imaging the tissue distribution of glucose in livers using a PARACEST sensor. Magn Reson Med. 2008; 60(5):1047–55. [PubMed: 18958853]
78. Louie AY, Hüber MM, Ahrens ET, Rothbächer U, Moats R, Jacobs RE, Fraser SE, Meade TJ. In vivo visualization of gene expression using magnetic resonance imaging. Nat Biotechnol. 2000; 18(3):321–5. [PubMed: 10700150]
79. Wu Y, Soesbe TC, Kiefer GE, Zhao P, Sherry AD. A responsive europium(III) chelate that provides a direct readout of pH by MRI. J Am Chem Soc. 2010; 132(40):14002–3. [PubMed: 20853833]

80. glucose cest
81. Dixon WT. Simple proton spectroscopic imaging. Radiology. 1984; 153(1):189–94. [PubMed: 6089263]
82. Vigneron DB, Nelson SJ, Murphy-Boesch J, Kelley DA, Kessler HB, Brown TR, Taylor JS. Chemical shift imaging of human brain: axial, sagittal, and coronal P-31 metabolite images. Radiology. 1990; 177(3):643–9. [PubMed: 2243963]
83. Behar KL, Petroff OA, Prichard JW, Alger JR, Shulman RG. Detection of metabolites in rabbit brain by ^{13}C NMR spectroscopy following administration of [1-^{13}C]glucose. Magn Reson Med. 1986; 3(6):911–20. [PubMed: 2881185]
84. Gruetter R, Novotny EJ, Boulware SD, Mason GF, Rothman DL, Shulman GI, Prichard JW, Shulman RG. Localized ^{13}C NMR spectroscopy in the human brain of amino acid labeling from D-[1-^{13}C]glucose. J Neurochem. 1994; 63(4):1377–85. [PubMed: 7931289]
85. Zhou J, Lal B, Wilson DA, Laterra J, van Zijl PC. Amide proton transfer (APT) contrast for imaging of brain tumors. Magn Reson Med. 2003; 50(6):1120–6. [PubMed: 14648559]
86. van Zijl PC, Jones CK, Ren J, Malloy CR, Sherry AD. MRI detection of glycogen in vivo by using chemical exchange saturation transfer imaging (glycoCEST). Proc Natl Acad Sci U S A. 2007; 104(11):4359–64. [PubMed: 17360529]
87. Middleton H, Black RD, Saam B, Cates GD, Cofer GP, Guenther R, Happer W, Hedlund LW, Johnson GA, Juvan K. MR imaging with hyperpolarized 3He gas. Magn Reson Med. 1995; 33(2): 271–5. [PubMed: 7707920]
88. Mugler JP 3rd, Driehuys B, Brookeman JR, Cates GD, Berr SS, Bryant RG, Daniel TM, de Lange EE, Downs JH 3rd, Erickson CJ, Happer W, Hinton DP, Kassel NF, Maier T, Phillips CD, Saam BT, Sauer KL, Wagshul ME. MR imaging and spectroscopy using hyperpolarized 129Xe gas: preliminary human results. Magn Reson Med. 1997; 37(6):809–15. [PubMed: 9178229]
89. Golman K, Olsson LE, Axelsson O, Månsson S, Karlsson M, Petersson JS. Molecular imaging using hyperpolarized ^{13}C. Br J Radiol. 2003; 76(Spec No 2):S118–27. [PubMed: 15572334]
90. Cudalbu C, Comment A, Kurdzesau F, van Heeswijk RB, Uffmann K, Jannin S, Denisov V, Kirik D, Gruetter R. Feasibility of in vivo ^{15}N MRS detection of hyperpolarized ^{15}N labeled choline in rats. Phys Chem Chem Phys. 2010; 12(22):5818–23. [PubMed: 20461252]
91. Witney TH, Kettunen MI, Day SE, Hu DE, Neves AA, Gallagher FA, Fulton SM, Brindle KM. A comparison between radiolabeled fluorodeoxyglucose uptake and hyperpolarized (13)C-labeled pyruvate utilization as methods for detecting tumor response to treatment. Neoplasia. 2009; 11(6): 574–82. [PubMed: 19484146]
92. Golman K, Zandt RI, Lerche M, Pehrson R, Ardenkjaer-Larsen JH. Metabolic imaging by hyperpolarized ^{13}C magnetic resonance imaging for in vivo tumor diagnosis. Cancer Res. 2006; 66(22):10855–60. [PubMed: 17108122]
93. Albers MJ, Bok R, Chen AP, Cunningham CH, Zierhut ML, Zhang VY, Kohler SJ, Tropp J, Hurd RE, Yen YF, Nelson SJ, Vigneron DB, Kurhanewicz J. Hyperpolarized ^{13}C lactate, pyruvate, and alanine: noninvasive biomarkers for prostate cancer detection and grading. Cancer Res. 2008; 68(20):8607–15. [PubMed: 18922937]
94. Day SE, Kettunen MI, Gallagher FA, Hu DE, Lerche M, Wolber J, Golman K, Ardenkjaer-Larsen JH, Brindle KM. Detecting tumor response to treatment using hyperpolarized ^{13}C magnetic resonance imaging and spectroscopy. Nat Med. 2007 Nov; 13(11):1382–7. Erratum in: Nat Med. 2007 Dec;13(12):1521. [PubMed: 17965722]
95. Gallagher FA, Kettunen MI, Day SE, Hu DE, Ardenkjaer-Larsen JH, Zandt R, Jensen PR, Karlsson M, Golman K, Lerche MH, Brindle KM. Magnetic resonance imaging of pH in vivo using hyperpolarized ^{13}C-labelled bicarbonate. Nature. 2008 Jun 12; 453(7197):940–3. [PubMed: 18509335]
96. Gallagher FA, Kettunen MI, Hu DE, Jensen PR, Zandt RI, Karlsson M, Gisselsson A, Nelson SK, Witney TH, Bohndiek SE, Hansson G, Peitersen T, Lerche MH, Brindle KM. Production of hyperpolarized [1,4-$^{13}C_2$]malate from [1,4-$^{13}C_2$]fumarate is a marker of cell necrosis and treatment response in tumors. Proc Natl Acad Sci U S A. 2009 Nov 24; 106(47):19801–6. [PubMed: 19903889]

97. Gabellieri C, Reynolds S, Lavie A, Payne GS, Leach MO, Eykyn TR. Therapeutic target metabolism observed using hyperpolarized ^{15}N choline. J Am Chem Soc. 2008; 130(14):4598–9. [PubMed: 18345678]

98. Gore JC, Yankeelov TE, Peterson TE, Avison MJ. Molecular imaging without radiopharmaceuticals? J Nucl Med. 2009; 50(6):999–1007. [PubMed: 19443583]

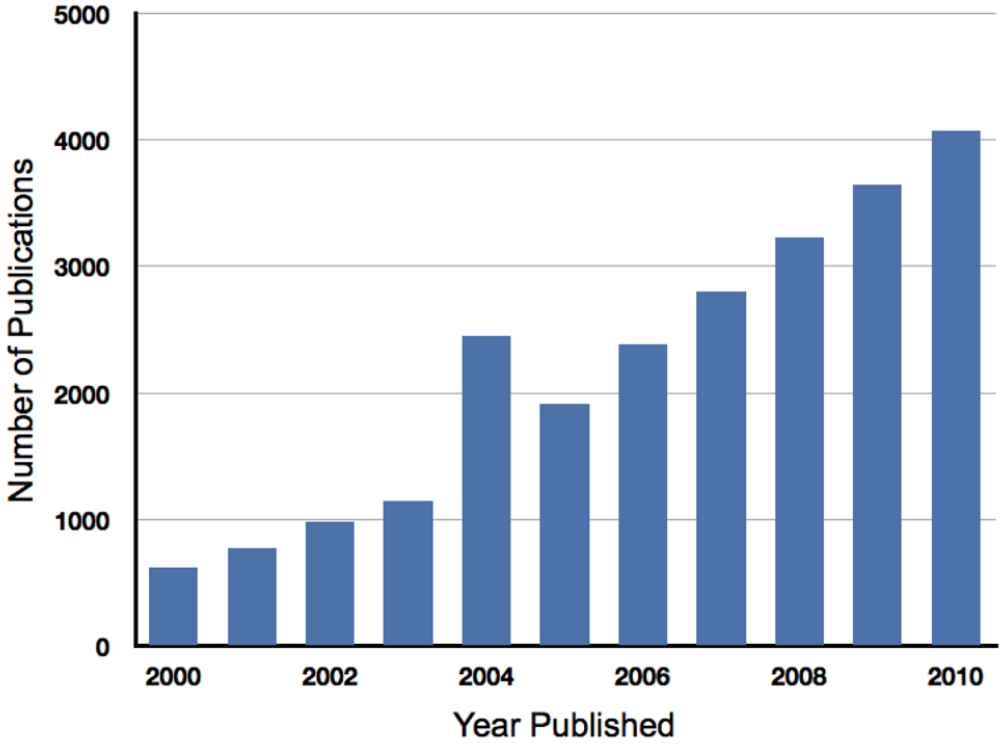

Figure 1.
The growth of molecular imaging in the past decade as measured by the number of publications each year reported in the PubMed database.

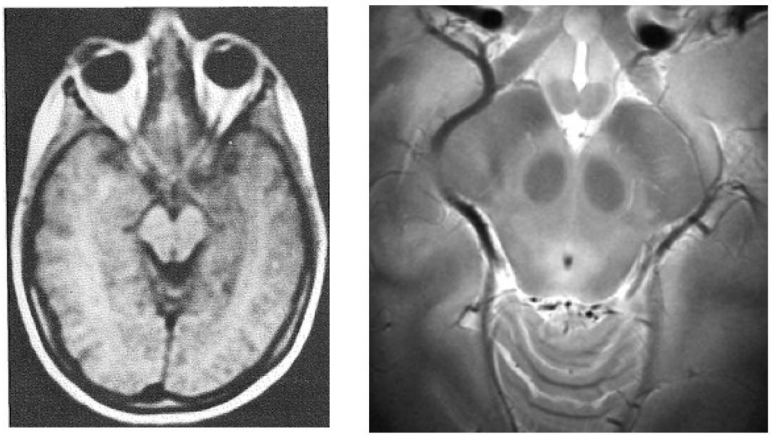

Figure 2.
(Left) Transaxial cross section of human brain acquired in 9 minutes at 0.15 Tesla in 1984 (voxel sizes ≈ 2 × 2 × 8 mm) (Right) part of the same mid-brain region imaged at 7 Tesla in 2008 in 4 minutes (voxel size 0.5 × 0.5 × 3 mm)

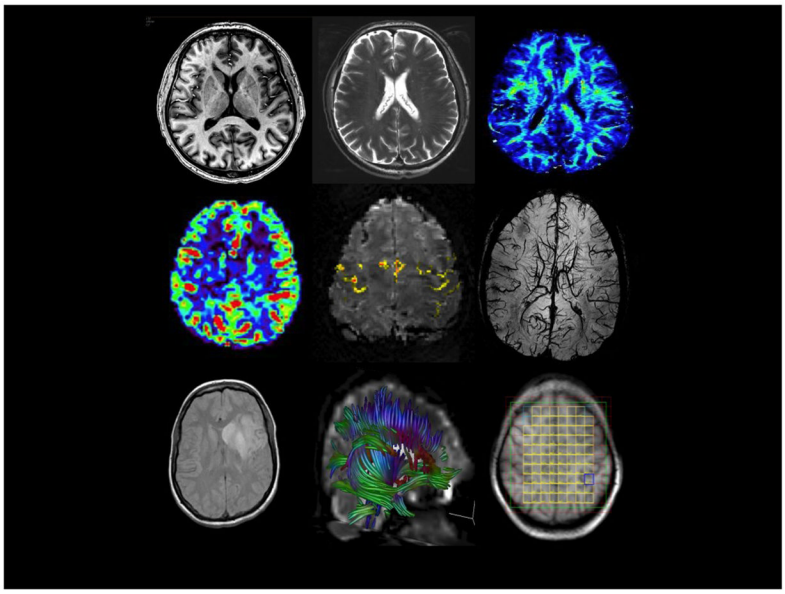

Figure 3.
a selection of different types of MR images produced by a standard, modern clinical scanner. From top to bottom, left to right these are (a) T1 weighted (b) T2 weighted (c) a map of quantitative magnetization transfer pool ratio (d) blood perfusion (e) a BOLD map of activation (f) a venogram (g) diffusion weighted (h) a DTI image of white matter tracts (i) multi-voxel high resolution MR spectra

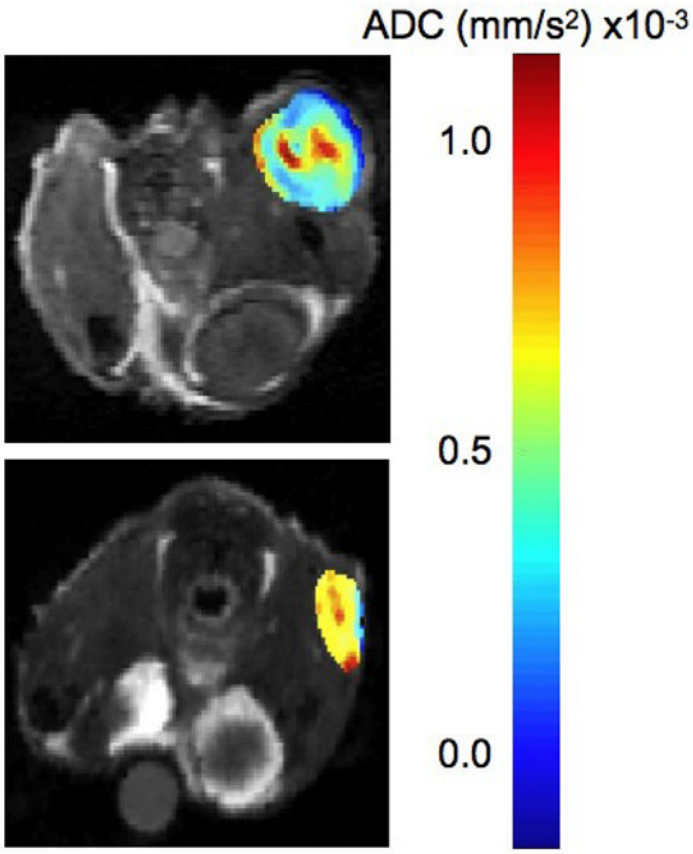

Figure 4.
ADC maps overlaid on T2-weighted images of a mouse model of HER2+ breast cancer treated with trastuzumab; (Top). at baseline and (Bottom) one week (two cycles) after treatment. Residual tumor ADC values generally increase after successful treatment with the drug.

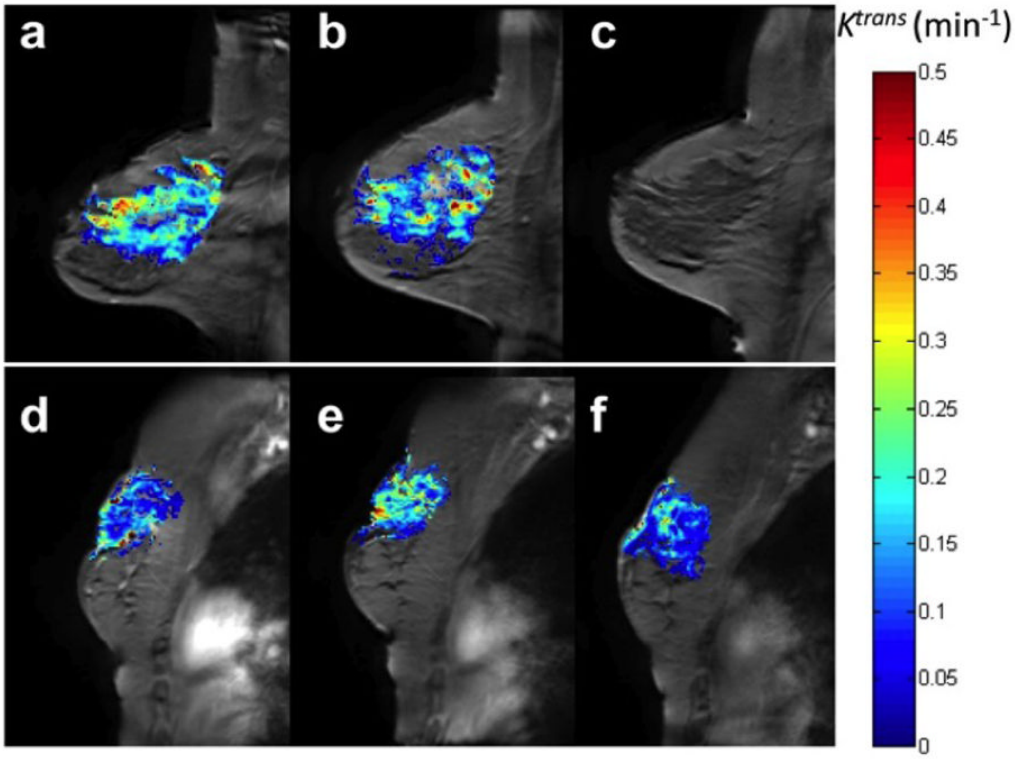

Figure 5.
DCE imaging of human breast cancer. (Top row) K^{trans} maps overlaid on T_1-weighted SPGRE image acquired before treatment (panel a), after one cycle of neoadjuvant chemotherapy (panel b) and at the conclusion of a therapy but prior to surgery. This is an example of patient showing a complete clinical response. (Bottom row) Similar data for a patient exhibiting progressive disease. In the top panel, there is a general decrease in K^{trans} values from pre- to post-one cycle of therapy (panels a and b, respectively), whereas in the bottom row there is a general increase (panels d to e) and this correlates with disease burden at the time of therapy.